

National Centre for Catalysis Research

(NCCR)

IIT Madras

An assignment on

- Dye sensitized solar cells and its current status
- Photo corrosion and its role in photoelectron chemical cells with typical examples

Submitted by

Mahboob Alam

CA12M004

To

Prof. B. Vishwanathan

Dye sensitized solar cells and its current status

Introduction

Nobel laureate Richard Smalley listed energy and environment problems on the top of challenges that we will face in next 50 years. The increase in energy consumption has accelerated the depletion of the earth's oil reserves, and the combustion exhaust of fossil fuels has resulted in the environmental contamination and greenhouse effect. Currently, worldwide concerns of such problems significantly spur the technological endeavor of renewable and green energy. The European Union (EU) has set a goal that by 2020 renewable energy should account for 20% of the EU's final energy consumption (10.3% in 2008). In accordance, the American Recovery and Reinvestment Act in the United States has budgeted more than \$80 billion in clean energy development aiming to reduce greenhouse gas emission by 28% by 2020. At present, a clear trend has been observed as the renewable energy share of global energy consumption in 2008 is 19%, which is a 50% increase compared to the 13% in 2003. Among all the renewable energy forms, solar energy has showed its advantages and potential for power generation. Solar radiation amounts to 3.8 million EJ/year, which is approximately 10,000 times more than current energy needs. From the perspective of energy conservation and environmental protection, it is desirable to directly convert solar radiation into electrical power by the application of photovoltaic devices. It is shown in Fig. 1, in the 5-year period between the end-2004 to 2009, solar photovoltaic energy generation has increased at 60% annual growth rate, fastest among all the renewable technologies.

High cost and complicated production process exclude traditional silicon-based solar cells from the domestic and other commercial applications. However, in recent decades several organic solar cells have been invented that combine the lightweight and flexibility of organic molecules with the low module cost. In terms of efficiency and easy fabrication, the dye-sensitized solar cell is one of the most promising alternatives to the silicon solar cells. In 1991, Oregan and Grätzel built the first dye sensitized nanocrystalline solar cells whose photoelectric energy conversion rate reached 7.1% and incident photon to electrical current conversion efficiency was approximately 80%. This simple structure and low cost technology have further stimulated great research interest to improve the efficiency of dye-sensitized solar cells which has attained ca. 10% a level deemed as necessary for commercial use.

Operational principle of the dye-sensitized solar cell

Dye-sensitized solar cell (DSSC) is a semiconductor photovoltaic device that directly converts solar radiation into electric current. The operational principle of DSSC is illustrated in Fig. 2. The system consists of the following:

- (i) A transparent anode made up of a glass sheet treated with a transparent conductive oxide layer;
- (ii) A mesoporous oxide layer (typically, TiO_2) deposited on the anode to activate electronic conduction;
- (iii) A monolayer charge transfer dye covalently bonded to the surface of the mesoporous oxide layer to enhance light absorption;
- (iv) An electrolyte containing redox media in an organic solvent effecting dye-regenerating; and
- (v) A cathode made of a glass sheet coated with a catalyst (typically, platinum) to facilitate electron collection

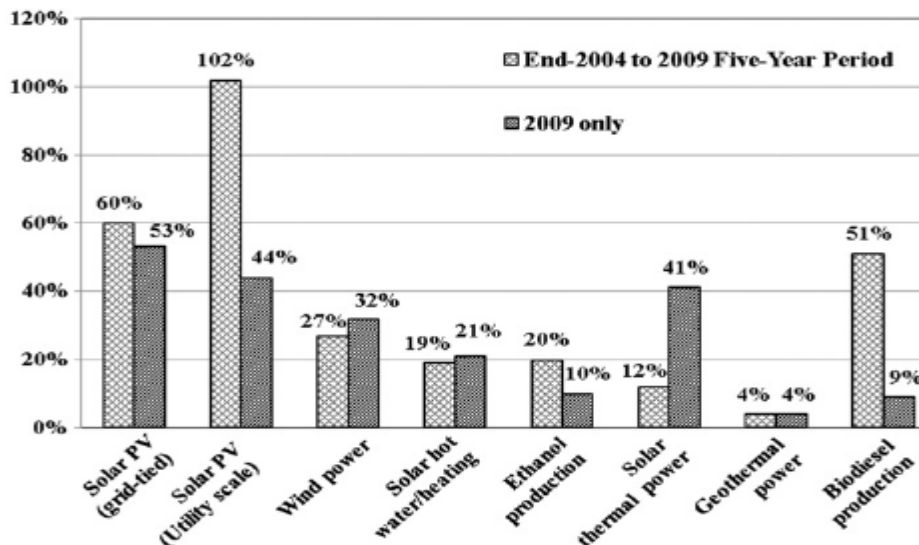


Fig.1 Average annual growth rates of renewable energy capacity, the end-2004–2009

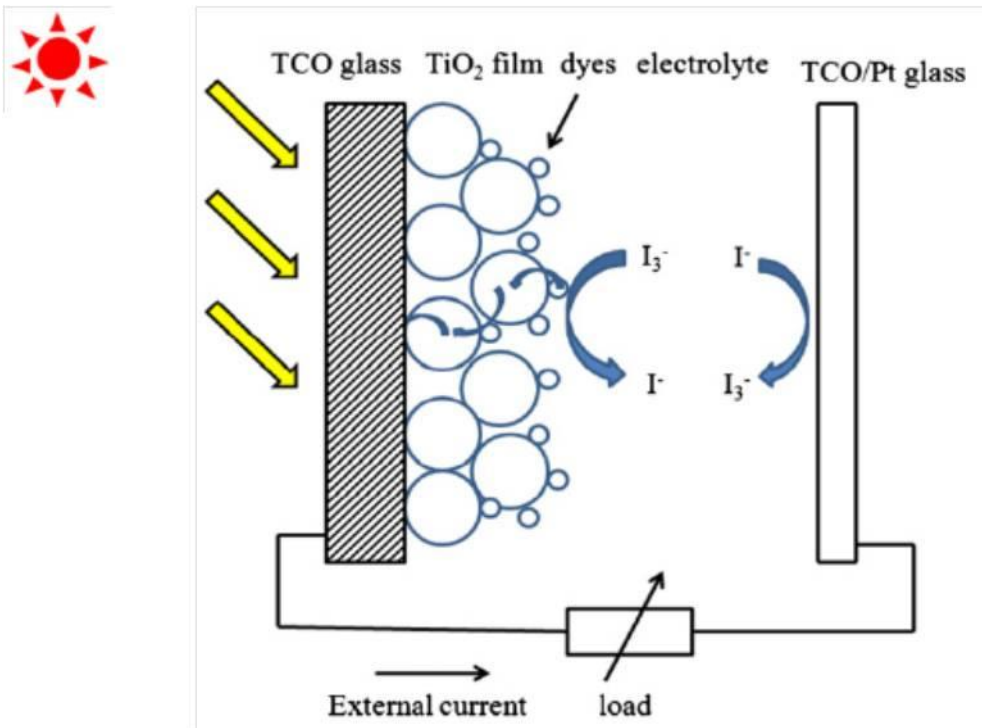


Fig 2. Schematic diagram of the dye-sensitized solar cell

When exposed to sunlight, the dye sensitizer gets excited from which an electron is injected into the conduction band of the mesoporous oxide film. The generated electrons diffuse to the anode and are utilized at the external load before being collected by the electrolyte at cathodes surface to complete the cycle. In order to enhance electrical conductivity and light transmittance, conducting glass is used as the substrate. There are mainly two types of conducting glass: indium-doped tin oxide (ITO) and fluorine-doped tin oxide (FTO). The standard to select a proper type is sometimes ambiguous because of the variety of cell configurations and materials. The semiconductor electrode is usually a layer of nano-crystalline titanium dioxide (TiO_2), a thin film deposited on the conducting glass film with the thickness of 5–30 nm, which plays an important role in both the exciton dissociation and the electron transfer process. The porosity and morphology of the TiO_2 layer are dominant factors that determine the amount of dye molecules absorbed on its surface which can provide an enormous surface area for the monolayer dye molecules to harvest incident light. A large number of artificial dye molecules have been synthesized since the first introduction of dye-sensitized solar cells and some of them have already been successfully commercialized such as N3, N719 and Z907. Desirable dye molecules have to meet certain criteria, such as match with the solar spectrum, long-term operational stability, and firm graft on the semiconductor surface. In addition, their redox potential should be high enough to facilitate the regeneration reaction with a redox mediator. As such, iodide and tri-iodide (I^-/I_3^-) redox couple is most commonly used in the liquid electrolyte, while other solid-state and quasi-solid electrolytes

like organic hole-transport material and polymer gel are also applicable Platinum is generally used as the cathode to catalyze the reduction of the oxidized charge mediator The overall performance of the above described solar cell can be evaluated interms of cell efficiency(η)and fill factor (FF) expressed as

$$FF = \frac{V_{max}J_{max}}{V_{oc}J_{sc}} \quad \text{.....} \rightarrow 1$$

$$\eta = \frac{V_{oc}J_{sc}}{P_{in}} \times FF \times 100\% \quad \text{.....} \rightarrow 2$$

where J_{sc} is the short-circuit current density(mAcm⁻²), V_{oc} the open-circuit voltage(V),and P_{in} the incident light power. J_{max} and V_{max} correspond to current and voltage values ,respectively where the maximum power output is given In the J–V curve.

In the band gap theory, the difference between the quasi Fermi level of the TiO₂ layer and the electrolyte redox potential determines the maximum voltage generated under illumination. As shown in Eq. (3) the open-circuit voltage varies with the iodide concentration because the recombination reaction occurs between the electrons on the conduction band of TiO₂ and I³⁻(tri iodide)

$$V_{oc} = \frac{kT}{q} \ln\left(\frac{\eta\Phi_0}{n_0k_{et}[I_3^-]}\right) \quad \text{.....} \rightarrow 3$$

where Z is the quantum yield of photo generated electron for the given incident photo flux(F_0); n_0 represents the electron density on the conduction band of TiO₂ in the dark, while k_{et} reflects the recombination reaction rate for the given tri iodide concentration .

$$J_{sc} = e \int IPCE(\lambda)\Phi_0(\lambda)(1-r(\lambda))d\lambda$$

Panchromatic sensitizer

As mentioned above, the ideal sensitizer has to meet several requirements that guide effective molecular engineering

(i) the sensitizer should be able to absorb all incident light below the near-IR wavelength of approximately 920nm ;

(ii) it must carry a carboxylate or phosphonate group to anchor on the surface of semiconductor oxide;

(iii) the lowest unoccupied molecular orbital (LUMO) of the sensitizer must match to the edge of the conduction band of the oxide to minimize the energetic potential losses during the electron transfer reaction during the electron transfer reaction;

(iv) the highest occupied orbital (HOMO) of the sensitizer must be sufficiently low to accept electron donation from an electrolyte or a hole conductive material;

(v) it should be stable enough to endure 10^8 turnovers corresponding to 20 years exposure to sunlight without apparent degradation

Since its discovery in 1993, cis-RuL₂-(NCS)₂ (N3 dye) has become the paradigm of the efficient charge-transfer sensitizer for nanocrystalline TiO₂ films. It has an absorption threshold around 800 nm covering the visible to the near-infrared region of solar spectrum. In addition, N3 dye can inject photo excited electrons into the semiconductor layer efficiently via carboxylate groups which on the one hand firmly attach to the surface of TiO₂ as an electron transfer channel, and on the other hand link to the bipyridyl moiety to lower the energy of the ligand π orbital. Since the molecular electronic transition is a metal-to-ligand charge transfer, this structure is energetically favored in the electron injection process. The performance of N3 dyes as a sensitizer is almost unmatched until the emergence of black dye. Nazeeruddin et al. first reported the synthesis of a class of black dye which displays the panchromatic sensitization character over the whole visible range extending from the near-IR region up to 920 nm. Later conversion efficiency utilizing black dye was certified to be 10.4% by the Swiss Federal Institute of Technology in Lausanne (EPFL). Recently, by using black dye N749, Chiba et al. [25] could achieve the highest recorded overall efficiency of approximately 11.1% with an area of 0.219 cm² [2] under standard AM 1.5 illumination. Until now, the photovoltaic performance of black dyes is expected to be superior to all other known charge-transfer sensitizers in terms of the whole range light absorption [26]. Incident photon to current conversion efficiency (IPCE) comparison between N3 and N749 is presented in **Fig. 3**. It is observed that the spectrum response of black dye extends ca. 100 nm wavelength to 900 nm the infrared region than that of N3 dye, which covers more near-IR region of the sunlight spectrum leading to a high IPCE value.

Though ruthenium (II) based dyes have provided a relatively high efficiency, there are several drawbacks of them: the high cost and the limited amount of noble metals, and also the sophisticated synthesis and purification steps. To address these issues, metal-free organic dyes have been prepared and applied in DSSCs to replace Ru (II) based dyes

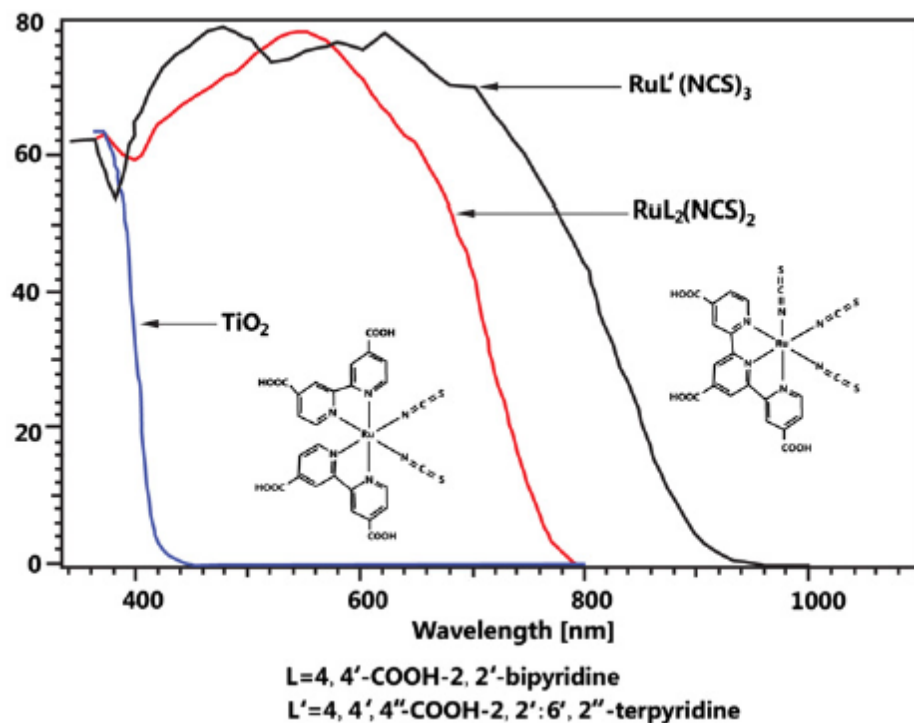


Fig.3. Incident photo to current conversion efficiency (IPCE): chemical structures of the sensitizers are shown as insets .

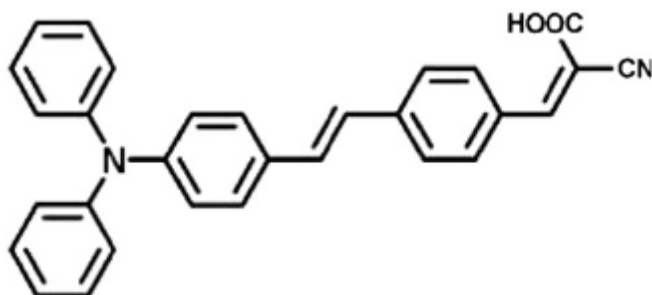


Fig.4. Molecular structure of TA-St-CA dye

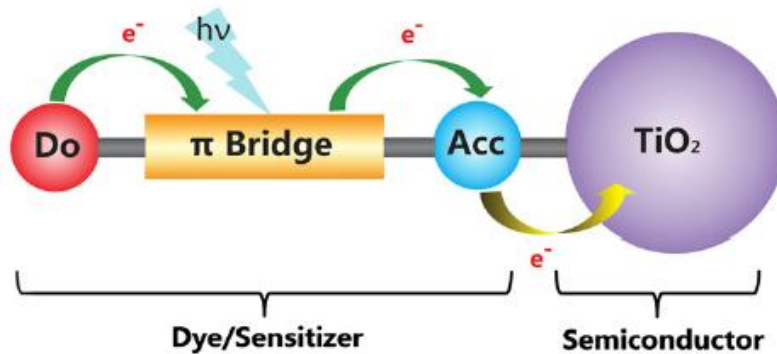


Fig.5.Designn structure of free metal organic dyes

Semiconductor photo anode

At present, an overall solar-to-energy conversion efficiency 9.1% has been obtained by Hwang et al. based on an organic metal-free dye TA-St-CA shown in Fig. 4. It contains a p-con- jugated oligo-phenylenevinylene unit with an electron donor– acceptor moiety for intra molecular charge transfer and a carboxyl group as an anchoring unit for the attachment onto TiO_2 nano –as an anchoring unit for the attachment onto TiO_2 nano- particles. This configuration can be generalized as the donor-pi bridge-acceptor structure shown in Fig. 5, which implies an essential design principle for metal-free dyes. Guided by this design design principle, Yella et al. synthesized a donor-p bridge- acceptor zinc porphyrin dye(YD2-o-C8) which suppresses the interfacial electron back transfe r from the nanocrystalline TiO_2 film to the oxidized cobal tmediator, and leads to a strikingly high power conversion efficiency of 12.3% under simulated air mass 1.5 global sunlight.

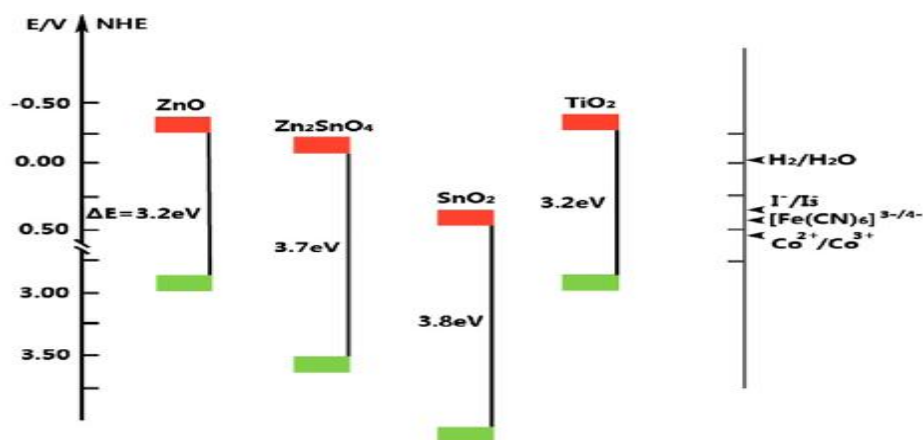


Fig.6.Band positions of several semiconductors and potentials of redox couples are represented using normal hydrogen electrode as reference

Fig. 6 shows that various semiconductor oxides have similar energy band structure as that of TiO_2 . The structure similarity makes them not only a possible substitute to TiO_2 in DSSCs, but also brings its own unique characteristic towards it. Intensive research has been dedicated to investigate this issue and potential application in other regimes. Zinc oxide (ZnO) is a promising alternative to TiO_2 because of the similar band structure and relatively high electron mobility ($1-5 \text{ cm}^2 \text{ V}^{-1} \text{ s}^{-1}$). Redmond et al. reported the first transparent nano-crystalline ZnO films prepared on a conducting glass substrate by sol-gel techniques. They are sensitized by cis-RuL₂-(NCS)₂ (N3 dye) and incorporated as the light-harvesting unit in a regenerative photo-electrochemical cell. The resulting device has a monochromatic IPCE of 13% at 520 nm and a simulated AM1.5 solar conversion efficiency of 0.4%. This low efficiency is mainly due to the dissolution of the ZnO surface and formation of Zn²⁺/dye aggregates in the acidic N3 solution. Later on, such obstacles are overcome by adding a base (KOH) to the acidic loading solution [36] or immersing the ZnO film in ethanolic solution under reflux. Currently, Saito and Fujihara [38] fabricated ZnO photo-anodes by a squeegee method and obtained the highest overall light-to-electric conversion efficiency of 6.58% under AM1.5 with a large short-circuit photo current density of 18.11 mA cm^{-2} .

Tin dioxide (SnO₂) is another attractive option having two main advantages over TiO_2 : high mobility, and large band gap. At room temperature (300 K), SnO₂ electron mobility (ca. $100-200 \text{ cm}^2 \text{ V}^{-1} \text{ s}^{-1}$) was measured by Fonstad and Rediker, which is three orders higher than that of TiO_2 (ca. $0.1-1 \text{ cm}^2 \text{ V}^{-1} \text{ s}^{-1}$). The larger band gap of SnO₂ (3.8 eV), compared to TiO_2 (3.2 eV), would create fewer oxidative holes in the valence band under ultraviolet illumination, thereby reducing the dye degradation rate and improving the long-time stability of DSSCs. More positive band edge position facilitates electron injection from photo-excited dye molecules. However, surprisingly the performance of dye-sensitized solar cells based on SnO₂ is so far much less than that based on TiO_2 . The inferior photo-voltaic properties of SnO₂ are ascribed to the faster electron recombination dynamics resulting from a 100-fold higher electron diffusion constant at matched electron densities, and from a 300 mV positive shift of the SnO₂ conduction band. In addition, the lower isoelectric point (IEP) of SnO₂ (pH 4-5), compared with TiO_2 (pH 6-7), inhibits the adsorption of dye molecules with acidic carboxyl groups [45]. To overcome the above issues, conformal isolating oxide layers such as TiO_2 , ZnO, MgO, and Al₂O₃ are coated on the surface of SnO₂ photoanode to suppress the back reaction, which can significantly improve the photo conversion efficiency. As reported by Senevirathna et al. [46], the maximum overall light-to-electrical efficiency of about 7% can be achieved by MgO-coated SnO₂ DSSCs.

Tan et al. [47] first synthesized large band gap energy (3.6 eV) ternary oxides Zn₂SnO₄ nano particles with desirable particle size from a hydro thermal process and tested it in the DSSCs. It could achieve an overall light-to-electrical conversion efficiency of about 3.8% under AM1.5 illumination. This efficiency is comparable to that of the single component ZnO solar cell (4.1%) and such Zn₂SnO₄ is more stable than ZnO against acidic dyes. Currently, the short electron diffusion length remains a limiting factor for the performance of Zn₂SnO₄ cells.

Transparent conducting substrate

Apart from semiconductor oxide film, the transparent conducting substrates also play an important role in dictating the DSSCs' performance. They are thin layer films that function as a current collector and a support of the semiconductor layer in DSSCs. They have two important features: the high optical transparency which allows natural sunlight to pass through to the beneath of the active material without unwanted absorption of the solar spectrum, and the low electrical resistivity which facilitates electron transfer process and reduces energy loss.

Indium tin oxide (ITO, In₂O₃:Sn) films exhibit an ideal transparency (transmittance over 80%) and resistivity (ca. 10⁴ Ω cm) at room temperature, so they are widely used as transparent conducting oxide in the field of optoelectronic device. It is notable that depending on the preparation method, the electrical properties of ITO films disperse widely. As reported by Tahar In₂O₃:Sn synthesized from In₂(SO₄)₃ · nH₂O and SnSO₄ by dipping method has the resistivity of 6–8 × 10⁴ Ω cm. The low resistivity is believed to be the result of the large free carrier densities caused by (i) substitution of indium atom by tin atom releasing one extra electron, and (ii) oxygen vacancies acting as two electron donors. However, their low resistivity property could be deteriorated during the calcinations process in the DSSCs fabrication.

Typical fabrication of the photo electrodes in DSSCs involves coating and sintering TiO₂ pasta on conducting substrates at high temperature ca. 450 °C to improve the electronic contact. When ITO film is exposed to high temperature above 300 °C, the sheet resistance increases drastically, leading to very low device efficiency. Such increased resistance can be explained by the reduced carrier density. When ITO films annealed at a high temperature, oxygen in the atmosphere starts to fill the oxygen vacancies which function as an electron supplier.

To prevent the loss of charge carriers in high temperature, a double layer structure has been utilized to achieve the thermal stability of ITO-based substrates. The thin layer metal oxides, such as ATO (SnO₂:Sb antimony-doped tin oxide), AZO (aluminum-doped zinc oxide), and SnO₂ have been sputtered on to the ITO surface to form the double layer which has proved to be a much better structure than single layer ITO.

Apart from the listed transparent conducting oxides, fluoride-doped tin oxide (SnO₂:F, FTO) with a similar structure and working principle as ITO has been attempted. FTO-coated glass substrates have 70–80% transmittance in the visible range at a thickness of 750 nm, approximately 10% less than that of ITO substrates.

Studies have been conducted to compare the performance of ITO and FTO based DSSCs by Sima et al. They fabricated DSSCs in a standard configuration and TiO₂/TCO/glass layers were subjected to thermal treatment at 450°C for 2h in an oxygen atmosphere. It was found that the sheet resistance value of ITO increased from the original 18 Ω to 52 Ω after the thermal treatment, whereas sheet resistance of FTO remained unchanged at the value of 8.5 Ω.

Although widely used, the traditional ITO and FTO based transparent conducting oxide appears to be increasingly problematic due to the following:

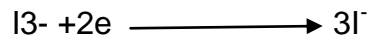
- the limited availability and high cost of the rare earth element indium,
- their sensitivity to thermal treatment and pH environment,
- their limited transparency in the near-infrared region, and mechanical brittleness.

Contact optimization

The three phase contact between ITO, TiO₂, and electrolyte in DSSCs plays a crucial role in photoelectron transfer and recombination dynamics. It is clear that the transport of extracted photoelectron in TiO₂ conduction band has to be transferred effectively to the ITO substrates in order to affect high cell efficiency. Therefore, methods have to be established to suppress the electron recombination during the transfer process.

There are mainly two recombination mechanisms: the electrons recombine with the holes in the excited dye molecules; and the electrons reduce the triiodide to iodide ion. In fact, these two chemical reactions occur concurrently as competing reactions. Research has been done to compare their reaction kinetics with the photoelectron

injection process. It was found that recombination between photoinjected electrons with oxidized dye molecules or I_3^- occurs in microseconds (10^{-6} s) Asbury et al. observed that the electron transfer dynamics between the excited dye molecules into the TiO_2 conduction band is on the femto second (10^{-15} s) scale by femto second mid-IR spectroscopy, whereas I^- ions reduce the oxidized dye on 10^{-8} seconds scale. Because the reduction rate of dye molecules is two orders of magnitude faster than the recombination with photoelectrons, the contribution of the former mechanism can usually be neglected. The dominant recombination reaction is represented by the reaction:



Because the electrolyte can penetrate through the mesoporous TiO_2 layer all the way to the ITO substrates, back electron transfer occurs on surface of both TiO_2 and ITO substrate. One of the successful approaches to suppress the detrimental recombination is to develop a blocking layer on the oxide electrode material.

There exist various types of blocking layers made of semiconductors and insulating materials such as TiO_2 , Nb_2O_5 , ZnO , $CaCO_3$ and $BaCO_3$. They are tested for their effectiveness in the DSSCs. Among them, the compact TiO_2 layer seems to be the most suitable candidate because it not only alleviates the back electron transfer on the FTO surface, but also provides a larger contact area between TiO_2 /FTO to enhance the electron transfer as shown in Fig. 7.

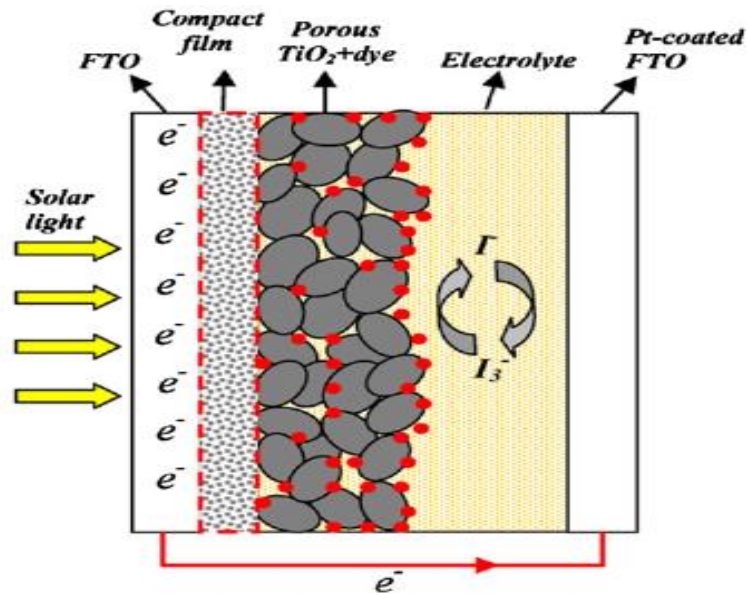


Fig. 7. Schematic diagram of the DSSC with a compact TiO_2 layer

It is commonly assumed that the back electron transfer on the FTO substrate can be neglected under short-circuit condition because the I_{3^-} to I^- exchange current density is negligibly small. The major electron recombination takes place on the surface of TiO_2 mesoporous network because its surface area is much larger than that of FTO. Fortunately, suppression of back electron transfer in TiO_2 has been achieved by passivating recombination centers with 4-tertbutylpyridine

Morphology influence

Mesoporous films

Mesoporous materials have pores between 2 and 50 nm in diameter. They usually have a continuous network that can either be ordered or disordered resulting in high internal surface area. Such structure is favorable in heterogeneous chemical reactions because it provides a sufficient surface as reaction sites and facilitates mass diffusion by internal channels. The first dye-sensitized solar cells (DSSCs) based on the mesoporous TiO_2 films achieved a remarkable breakthrough. Till recently, the mesoporous film is regarded as the most favorable electrode structure and widely used as a standard to study DSSCs.

Unique characteristics are found in mesoporous TiO_2 compared with its compact analogs: the low inherent film conductivity, no built-in electrical field within nanocrystalline particles, and three dimensional semiconductor/electrolyte interface contact. Mesoporous film, though it yields extremely high specific surface area for dye uptake, could enhance the charge recombination to triiodide ions on the TiO_2 /electrolyte interface. Thus, it is advantageous to have thinner films.

The mesoporous structure of the film depends on the preparation method, and its pore size distribution can be adjusted, for example, by controlling molar ratio of stearic acid to titanium tetra isopropoxide as precursor [64]. Barbe´ et al. studied the microstructure of the mesoporous film correlation with preparation conditions such as precursor chemistry, temperature for hydrothermal growth, binder addition, and sintering conditions influence. The film morphology and network geometry have a great influence on the electron transport dynamics of DSSCs. The correlation between film morphology and photo electro chemical performance of DSSCs was investigated by Saito et al. [66]. It is reported that the amount of dyes adsorbed and photocurrent generated under illumination were proportional to the roughness factor (R_f).

High order nanostructure

the conductivity of mesoporous film is much lower than its bulk analog. The electron diffusion coefficient determined by laser flash-induced transient photocurrent measurement [69] and intensity modulated photocurrent spectroscopy is more than two orders of magnitude smaller than the value for bulk anatase crystal. This puzzling phenomenon is due to the network defects which results in trapping/detrapping of electrons within grain boundaries, and can be predicted using the "Multiple trapping" model. Therefore, replacing TiO_2 nano particles with highly ordered nanostructure is expected to achieve a rapid electron transfer by minimizing the crystal trapping sites. Recently, it has been shown that the DSSCs based on the ordered arrays of TiO_2 or other metal oxide like ZnO manifest efficient charge separation and electron transfer feature

Adachi et al. reported a network structure of single-crystal like TiO_2 nanowires formed through surfactant-assisted processes at a low temperature (353K). The direction of crystal growth was controlled by changing the adsorption of surfactant molecules on the TiO_2 surface. A single-crystalline anatase exposing mainly the plane exhibits excellent ruthenium dye adsorption, four times higher as compared to commercial product P-25, thus leading to a high overall cell efficiency of 9.3%.

Law et al. [34] prepared zinc oxide (ZnO) nanowire arrays and first applied them to the DSSCs in 2005. ZnO nanowire arrays were formed according to the solution (ethanol) based process in which they adopted a modified seeded growth process to have a yield of long wires. In their study, a 10–15 nm thick film of ZnO quantum dots was deposited onto FTO substrates by dip-coating. Nano wires grew from these nuclei through the thermal decomposition of a zinc complex. It is found the use of poly-ethylenimine (PEI), a cationic polyelectrolyte, has a striking effect as it hindered the lateral growth to increase the wire length. In this array, wire length and diameter varied from 16 to 17 μm and 130 to 200 nm, respectively. The prepared ZnO nano wire films are excellent conductors.

Recently, Lei et al. fabricated large-scale, non curling anatase crystalline TiO_2 nanotube arrays on a FTO substrate via a four step process: (i) fabrication of TiO_2 nanotube on Ti foil by anodization, (ii) detachment of the amorphous free-standing TiO_2 nanotubes via ultrasonic treatment, (iii) transfer and adhesion to FTO substrates, and (iv) two-step annealing treatment. For a 20.8 mm length array, an overall photoconversion efficiency of about 8.1% can be achieved.

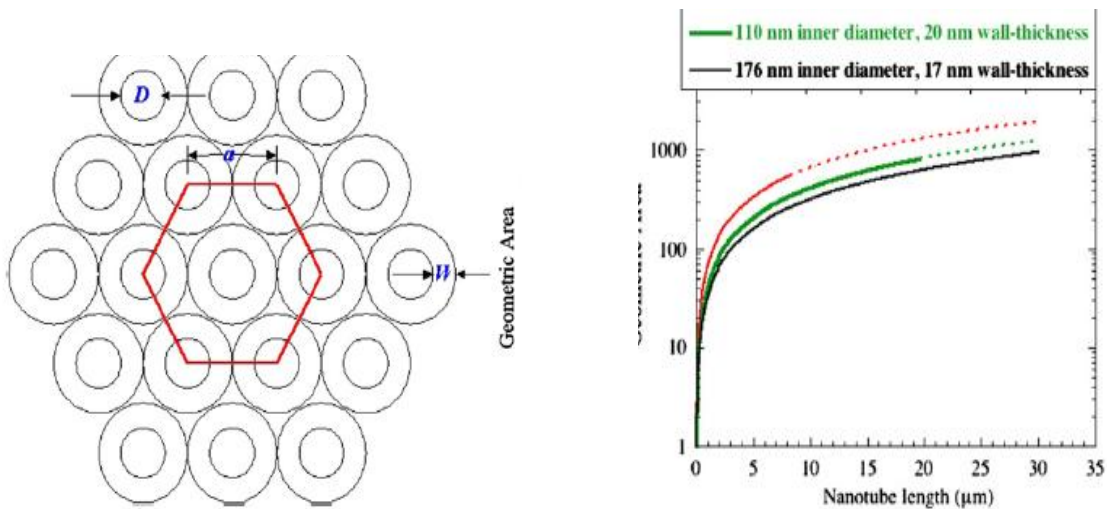


Fig. 8. (a) Idealized unit cell of TiO_2 nanotube array with inner diameter D , wall thickness W , and $a \approx \frac{1}{4}D + W$ and (b) geometric roughness factor Vs nano tube length

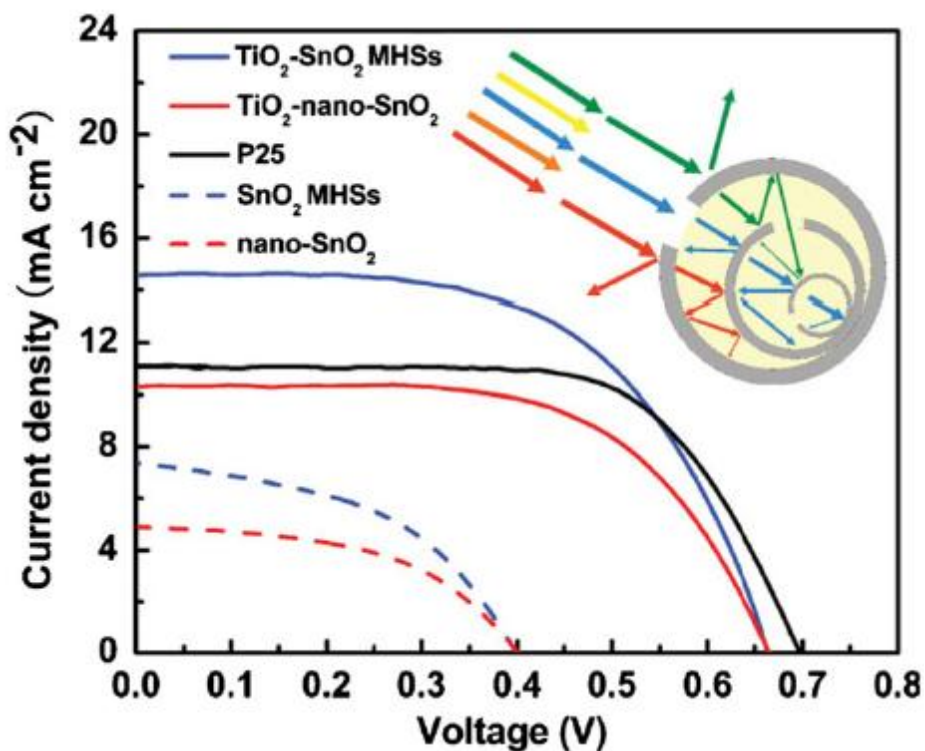


Fig 9. J-characteristics of DSSCs for different photoelectrode films (The inset illustrates the multiple reflecting and scattering of light in the multi layered hollow spheres.)

Electrolyte development

The electrolyte is a key component of all dye-sensitized solar cells (DSSCs). It functions as charge carriers collecting electrons at the cathode and transporting the electrons back to the dye molecule. In terms of the cell efficiency, the most popularly used electrolyte is the iodide/tri iodide (I^-/I_3^-) redox couple in an organic matrix, generally acetonitrile. However, there exist undesirable intrinsic properties which are inherent of a liquid electrolyte significantly affecting a device's long-term durability and operational stability. For example, not only the leakage of toxic organic solvent will cause environmental contamination, but also the evaporation of volatile iodine ions will increase the overall internal resistance by lowering concentration of the charge carrier. To overcome these disadvantages, research has been conducted to develop non-traditional electrolytes e.g. room temperature ionic liquids (RTILs), quasi-solid state and solid state electrolytes.

Liquid electrolyte

The most commonly used liquid electrolyte, namely iodide tri iodide (I^-/I_3^-), works well mainly due to its kinetics as shown in Fig. 10. The electron injection into the TiO_2 conduction band occurs in the femtosecond time range which is much faster than the electron recombination with I_3^- , and the oxidized dye preferably reacts with I^- than combining with the injected electrons. In the electrolyte, the I_3^- diffuses to cathode to harvest electrons and in turn produce I^- which diffuses in the opposite direction towards the TiO_2 electrode to regenerate dye molecules. The diffusion coefficient of I_3^- ions in the porous TiO_2 structure is about $7.6 \times 10^{-6} \text{ cm}^2/\text{s}$.

One important issue to be considered when using the I^-/I_3^- redox couple is its concentration. At low iodine concentration, it is difficult to maintain sufficient electrolyte conductivity and rapid redox reaction. On the other hand, when iodine concentration is high, electron recombination at the TiO_2 interface deteriorates the performance of DSSCs and meanwhile the rate of light absorption by redox couple is increased [86]. The exact quantitative relationship is expressed in Eq.(3) which shows that electron recombination processes determine the open circuit voltage (V_{oc}) which depends on the concentration of triiodide in the TiO_2 .

It is found that recombination can be suppressed by introducing additives to the electrolyte such as 4-tert-butylpyridine (4TBP), guanidiumthiocyanate [88], and methylbenzimidazole (MBI) [89]. These additives can improve the efficiency and stability, though they do not participate in the fundamental photoelectrochemical processes. The most probable mechanism is that these additives when absorbed by the TiO_2 surface block the reduction sites to keep electron acceptor molecules away from contact. A similar phenomenon was observed by Zhang et al. [90] when adding co-adsorbents in a dye bath.

In theory, the maximum voltage generated in DSSCs is determined by the difference between the quasi-Fermi level of the TiO_2 and the redox potential of the electrolyte, about 0.7 V under solar illumination conditions. In order to obtain a higher open circuit voltage and circumvent the corrosion of I^-/I_3^- redox couple, a variety of alternative redox couples have been introduced to DSSCs such as Br^-/Br_3^- , $SCN^-/(SCN)_2$, $SeCN^-/(SeCN)_3^-$, $Fe(CN)_6^{3-}/4^-$ [91] and Co(II)/Co(III) complex. Recently, Wang

et al. reported a new disulfide/thiolate redox couple that has negligible absorption in the visible spectral range and achieved an unprecedented efficiency of 6.4% under standard illumination test conditions. This novel redox couple set a new benchmark for iodide-free DSSCs by offering a viable pathway to scale up and practical applications. The best alternative redox couple to date seems to be cobalt poly pyridine complexes, because of their weak visible light absorption, the higher redox potential and the less aggressive corrosiveness towards metallic conductors. Recent research has proven that by tuning their redox potential to match the oxidation potential of the sensitizer can minimize the energy loss in the dye regeneration step and leads to attainment of strikingly high open-circuit voltage approaching 1 V.

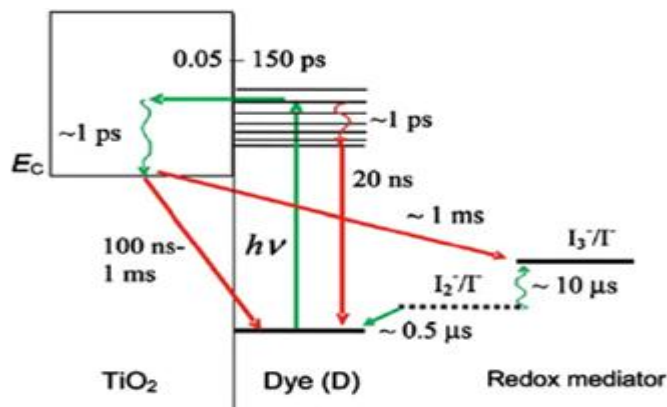


Fig.10. Kinetics of the cisRu(dcbpy)2(NCS)2 sensitized TiO2 solar cell with I-/I3- redox mediator

Solid-state electrolyte

A solid-state electrolyte is considered to be an alternative to the liquid electrolyte, because it could achieve a better mechanical stability and simplified fabrication processes. It is an essentially simple idea that replaces the liquid electrolyte with inorganic p-type semiconductors or organic hole transporting materials to eliminate the evaporation and leakage of liquid electrolyte. In this sense, the n-type semiconductor and p-type sensitizer make dye-sensitized solar cells inevitably analogous with traditional Si-based p-n junction solar cells in principle. A suitable hole-transport material must have a band gap structure compatible with the highest occupied molecular orbital (HOMO) level of the dye and the conduction band of TiO_2 to drive the charge-transfer process. The main difficulty in realizing such a solid-state electrolyte device is to form an intimate contact at the p-n junction interfaces.

The first p-type semiconductors acting as hole-transport materials were CuSCN and CuI, introduced by Tennakone et al. [100] and O'Regan and Schwartz. In their first step, they could achieve an overall efficiency less than 1%, due to the formation of unfilled voids in the TiO_2 inter-crystallite. During the deposition process, p-CuI crystalline semiconductors experience a rapid crystal growth. The formation of a crystal with a dimension exceeding that of TiO_2 pores will interfere with the filling process, leaving a large portion of pores unfilled. Later Kumara et al. found an effective crystal growth inhibitor triethylamine hydrothiocyanate (THT) to improve the cell efficiency to 3.75%. Recently, a novel working electrode $TiO_2/CuI/Cu$ was reported by Heng et al.

Future prospectus

Dye sensitized-solar cell (DSSC) has proven its potential as a cheap alternative to expensive silicon solar cells. It is a cost-effective technology that features relatively high efficiency, long-term stability and easy fabrication. In addition, DSSCs are more sensitive than crystalline silicon cells to visible light, and light incident at a shallow angle. Such characteristics enable DSSCs to be a reliable power source in low light intensity environment. Currently, DSSCs are still under laboratory research and development stage. Much work remains to be conducted to further improve its energy conversion efficiency for practical applications. Dyes, as a key component of DSSCs, have been receiving intensive research attention, because the light-to-electrical conversion of DSSCs strongly depends on the light absorption of sensitized dyes. Comprehensive studies aiming at synthesizing panchromatic dyes have been conducted for decades. However, as a general rule, dyes that absorb strongly do not typically exhibit broad absorption.

Recently, Hardin et al. [108] presented a new design where high-energy photons are absorbed by highly photoluminescent chromophores unattached to the titania and undergo Förster resonant energy transfer to the sensitizing dye. Different from co-sensitized technology, this novel architecture offers an alternative pathway to increase light harvesting in DSSCs.

Besides enhancing the performance, how to lower materials cost is another important issue that needs to be addressed in the future work. Wang and Kerr attempted to use paper as substrate to make flexible DSSCs (efficiency 2.66%). Although the Ni coated paper substrate is prone to crack generated in calcinations, the mature coating technology of paper substrate can provide an opportunity for low cost roll to roll mass production. The expensive metal platinum is used as electro catalyst on the cathode in DSSCs, and the necessary amount of platinum is ca. 10–100 mg/cm². In order to lower the materials' cost and obtain a good optical transparency, various noble metal-free materials are prepared and tested to examine their compatibility in DSSCs. Recently, Wang et al. [110] reported that CoS (cobalt sulfide nanoparticles deposited electrochemically on the flexible ITO/ PEN film, match the performance of Pt as a triiodide reduction catalyst in DSSCs. Remarkably, the cost of cobalt is several hundred times lower than that of platinum. Kavan et al. fabricated semi transparent (48.5%) thin films on F-doped SnO₂ (FTO) using commercial graphene nanoplatelets. Such graphene cathode exhibits comparable performance with the Pt cathode in ionic liquid based DSSCs. Moreover, this optical transparency is an essential feature that extends certain applications to tandem cells, windows and roof panels.

Apart from improving the performance of single component in DSSCs, tandem pn-DSSC is another option for further endeavors. Tandem cells combining the p-type DSSCs with typical n-type DSSCs could achieve a much better efficiency than single-junction DSSC, because it can harvest natural light more effectively by using spectral complementary dyes. Recently, Nattestad et al. designed a series of donor–acceptor dyes which comprise a variable-length oligothiophene bridge to control over the spatial separation of photogenerated charge carriers. It was found that such dyes significantly decelerated charge recombination in p-type DSSC and achieved an absorbed photon to electrons efficiency up to 96%.

Table 1

The highest efficiency achieved based on the different semiconductor materials.

Process	Composition	μ_{H1} ($\text{cm}^2\text{V}^{-1}\text{s}^{-1}$)	V_{oc} (V)	J_{sc} (mA cm^{-2})	FF	η (%)
Hydrothermal	Zn_2SnO_4		0.62	9.3	0.66	3.8 [47]
Squeegee method	ZnO		0.62	18.11	0.59	6.6 [38]
Surface spray	MgO/SnO ₂	100-200	0.75	14.21	0.67	7.2 [46]
Screen-printing	TiO ₂	0.1-1	0.74	20.9	0.72	11.1 [25]

Conclusion

As a novel photovoltaic technology, dye-sensitized solar cells (DSSCs) have potential to compete with traditional solar cells. Materials such as TiO_2 used in DSSCs are generally inexpensive, abundant and innocuous to the environment. Compared with silicon solar cells, they are insensitive to impurities in fabrication process, which accelerates a transition from research laboratory to mass production line. From the perspective of application, low weight and flexibility of DSSCs are desirable for the portable electronic device. It is found that DSSCs work better than silicon solar cells in the darker condition, for example, in the dawn and dusk, and also the overall efficiency is not seriously affected in the high temperature. In addition, the transparency and varied color of DSSCs could be utilized for decorative purposes like windows and sunroof. Up to now, such benefits have attracted considerable company investment and government funding. It is believed that with consistent efforts, DSSCs will be a reliable electrical power supplier in the future (Table 1).

Reference

- 1: Nobuyuki H. Renewable energy: RD&D priorities: insights from IEA technology programmes; 2006.
- 2: Gong jiewie. Jing Liang. Sumathy k. Fundamental concepts and novel materials on dye-sensitized solar cells (DSSCs)
- 3: Hassan MA, Sumathy K. Photovoltaic thermal module concepts and their performance analysis: a review. Renewable and Sustainable Energy Reviews 2010; 14(7):1845–59.

Photo corrosion and its role in photoelectron chemical cells with typical examples

Introduction

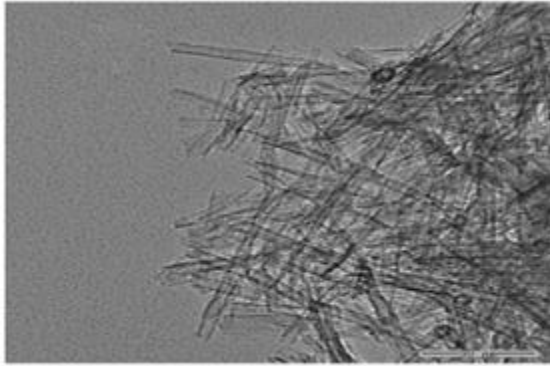
Silver carbonate (Ag_2CO_3) is unsuitable for photo catalyst, because it is liable to photo-corrosion that can seriously deactivate photocatalytic performance. Surprisingly, several recent publications state that Ag_2CO_3 possesses visible light photocatalytic behavior. For example, Xu et al. reported in 2011 that Ag_2CO_3 prepared by a precipitation method displays a high activity towards degradation of phenol and methylene blue under visible light irradiation. Since 1 year, Dai et al. prepared Ag_2CO_3 by a simple precipitation reaction between NaHCO_3 and AgNO_3 , aiming to reveal the photo-corrosion mechanism of Ag-based photocatalysts. Based on the plane-wave-based density functional theory, Dong et al. theoretically calculated the band gap of Ag_2CO_3 photocatalyst and proposed that Ag_2CO_3 photo-catalyst belongs to indirect band gap semiconductor. Besides, other Ag-containing photocatalysts such as Ag@AgCl , Ag@AgBr , Ag_2SO_3 , Ag_3PO_4 , silver vanadates, and AgMO_2 ($M = \text{Al}, \text{Ga}, \text{and In}$) might be promising high-efficient photocatalysts. These Ag-based photocatalysts, however, usually experience photo-corrosion under visible light irradiation, which causes damage to their photocatalytic activity. Thus, it is imperative to develop novel visible-light-active Ag_2CO_3 -based photocatalysts with excellent stability and high visible light photocatalytic activity.

Nanotubular titanate (denoted as NTA) can be well adopted as the precursor to fabricate highly visible-light-active photocatalysts. It was proposed that the generation of SETOVs accounts for the apparent visible light absorption rather than visible light photocatalytic activity of as-obtained anatase $\text{TiO}_2(\text{Vo})$ matrix. However, anatase $\text{TiO}_2(\text{Vo})$ doped with N shows visible light photocatalytic activity towards air pollutant, which is ascribed to the synergistic effect between SETOVs and doped-N.

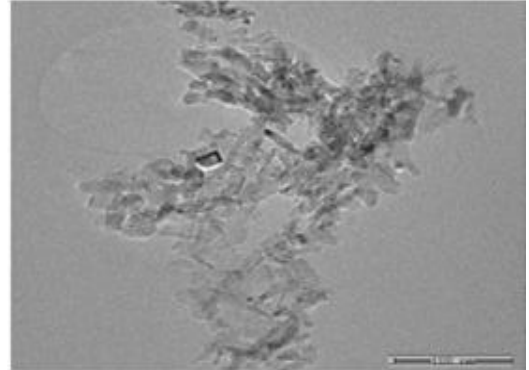
Bearing those perspectives in mind and viewing the important role of SETOVs in inducing visible light photocatalytic activity, in this paper $\text{Ag}_2\text{CO}_3/\text{TiO}_2(\text{Vo})$ was prepared using NTA as medium via a facile precipitation method. We aim in this paper to increase the stability of Ag_2CO_3 as a photocatalyst and improve the visible light photocatalytic activity of $\text{TiO}_2(\text{Vo})$ by making use of possible synergistic effect between Ag_2CO_3 and anatase $\text{TiO}_2(\text{Vo})$ matrix.

Results and discussion

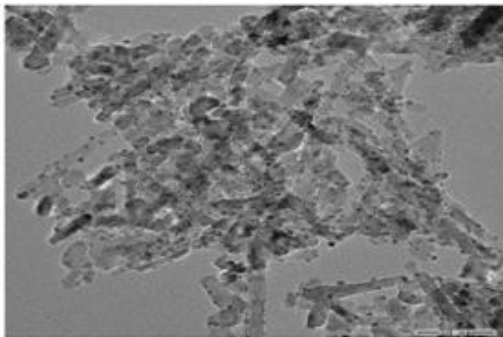
Fig1(a-c) shows the TEM morphologies of NTA, $\text{TiO}_2(\text{V}_o)$, and $\text{Ag}_2\text{CO}_3/\text{TiO}_2(\text{V}_o)$ samples, respectively. NTA have open-ended nanotubular morphology with a length of several tens of nanometers. After NTA were thermally treated at 600°C for 2h the resultant samples $\text{TiO}_2(\text{V}_o)$ do not remain the nanotubular morphology but were destroyed into nanorods with a diameter of ca. 50 nm. As can be seen from Fig. 1(c), Ag_2CO_3 rounded grains with a small diameter (ca. 2–5 nm) were uniformly dispersed on the surface of $\text{TiO}_2(\text{V}_o)$ samples. Furthermore, all the Ag_2CO_3 rounded grains were firmly attached to the surface of $\text{TiO}_2(\text{V}_o)$ samples, indicating the better incorporation between Ag_2CO_3 and $\text{TiO}_2(\text{V}_o)$ samples.



a)



b)



c)

Fig.1. TEM morphology of a)NTA b) $\text{TiO}_2(\text{V}_o^*)$, c) $\text{Ag}_2\text{CO}_3/\text{TiO}_2(\text{V}_o^*)$

Fig. 2 shows the XRD patterns of NTA, TiO₂(Vo), Ag₂CO₃, and Ag₂CO₃/TiO₂(Vo). NTA belongs to orthorhombic system in terms of crystal structure, which is well elucidated elsewhere. After orthorhombic NTA is heated at 600 °C in air, it undergoes phase transition generating anatase TiO₂(Vo). Besides, the XRD peaks of Ag₂CO₃ can be indexed to monoclinic phase Ag₂CO₃ which is in agreement with that reported elsewhere and its high diffraction peak intensity implies that it has good crystallinity. Moreover, Ag₂CO₃/TiO₂(Vo) shows a miscible structure covering monoclinic phase Ag₂CO₃ and anatase phase TiO₂(Vo), in accordance with the TEM results of Fig. 1c.

The diffuse reflectance spectra of NTA, P25, Ag₂CO₃, and Ag₂CO₃/TiO₂(Vo) samples are comparatively given in Fig. 3. On the one hand, NTA and P25 have no visible light absorption due to their wide band gap. On the other hand, Ag₂CO₃ shows a broad absorption in the visible light region, and its absorption-edge emerges at 480 nm. As to indirect band gap semiconductor Ag₂CO₃, a plot of $(\alpha h\nu)^{1/2}$ versus the energy of absorbed light (i.e., $h\nu$) can be obtained according to the equation $\alpha h\nu = A(h\nu - E_g)^n$, where α , ν , A , and E_g are the absorption coefficient, light frequency, proportionality constant, and band gap, respectively ($n = 2$). Relevant results are shown in the inset of Fig. 3. By extrapolating the tangent line along the $h\nu$ axis, we can estimate that the band gap (E_g) of Ag₂CO₃ is 2.20 eV. After Ag₂CO₃ is combined with TiO₂(Vo), resultant Ag₂CO₃/TiO₂(Vo) exhibits stronger visible light absorption. It has been reported that TiO₂(Vo) possess obviously visible light absorption owing to the formation of SETOVs (see Fig. S1). As can be seen from Fig. S1, the SETOVs in Ag₂CO₃/TiO₂(Vo) are originated from TiO₂(Vo) substrate. We can therefore infer that both pristine Ag₂CO₃ and SETOVs contribute to the visible light absorption of Ag₂CO₃/TiO₂(Vo). As a result, Ag₂CO₃/TiO₂(Vo) sample possesses stronger visible light absorption than Ag₂CO₃ alone.

The photocatalytic degradation rate of propylene over Ag₂CO₃ and Ag₂CO₃/TiO₂(Vo) under visible light irradiation as a function of reaction time are comparatively shown in Fig. 4. Propylene is photodegraded as soon as the light ($\lambda > 420$ nm) is turned on, and the initial removal rate of propylene over Ag₂CO₃ and Ag₂CO₃/TiO₂(Vo) is up to ca. 69.9% and 90.4%, respectively. Unfortunately, the visible light photocatalytic activity of Ag₂CO₃ sample gradually declines with extending reaction time (e.g., it declines from 69.9% to less than 10% after 250 min irradiation).

This indicates that Ag_2CO_3 sample is unstable possibly due to photo-corrosion under visible light irradiation. Differing from Ag_2CO_3 , $\text{Ag}_2\text{CO}_3/\text{TiO}_2(\text{Vo})$ shows high and stable visible light photocatalytic activity through the whole reaction time. This means that combination with $\text{TiO}_2(\text{Vo})$ helps to efficiently utilize the photo-corrosion of Ag_2CO_3 thereby leading to greatly increased photocatalytic activity and stability of $\text{Ag}_2\text{CO}_3/\text{TiO}_2(\text{Vo})$ under visible light irradiation. Dai et al. reported that adding AgNO_3 favors to increase the stability of Ag_2CO_3 photocatalyst for the photocatalytic degradation of RhB because Ag/AgNO_3 possesses a lower electrode potential than $\text{Ag}/\text{Ag}_2\text{CO}_3$. In this sense, $\text{Ag}_2\text{CO}_3/\text{TiO}_2(\text{Vo})$ should be more attractive and competitive, since it possesses much better stability than Ag_2CO_3 even in the absence of externally added ingredients.

To shed light on the visible light photocatalytic activity as well as photo-corrosion mechanism of Ag_2CO_3 and $\text{Ag}_2\text{CO}_3/\text{TiO}_2(\text{Vo})$ samples, Ag Auger MNN XPS measurements are conducted to elucidate changes in the chemical state of Ag element before and after photodegradation experiments. Relevant results are given in Fig. 5. The peak at ca. 904.0 eV is assigned to the Ag MNN peak of Ag_2CO_3 , and that at ca. 901.4 eV is assigned to metallic Ag. What should be emphasized is that, after visible light irradiation, the Ag MNN peak of Ag_2CO_3 is drastically reduced and the peak of metallic Ag becomes predominant. This is just because Ag_2CO_3 is unstable and undergoes photo-corrosion under visible light irradiation, resulting in metallic Ag owing to reduction of Ag p (see Fig. 5a). Such a photo-corrosion can seriously deactivate Ag_2CO_3 as a photocatalyst as evidenced in Fig. 4. More importantly, although Ag_2CO_3 in $\text{Ag}_2\text{CO}_3/\text{TiO}_2(\text{Vo})$ is also liable to photo-corrosion (see Fig. 5b), $\text{Ag}_2\text{CO}_3/\text{TiO}_2(\text{Vo})$ retains almost unchanged photocatalytic activity under visible light irradiation (see Fig. 4). This means that there should be newly-formed visible light photocatalytic activity to compensate the photocatalytic activity loss of $\text{Ag}_2\text{CO}_3/\text{TiO}_2(\text{Vo})$ owing to the photo-corrosion of Ag_2CO_3 . In other words,

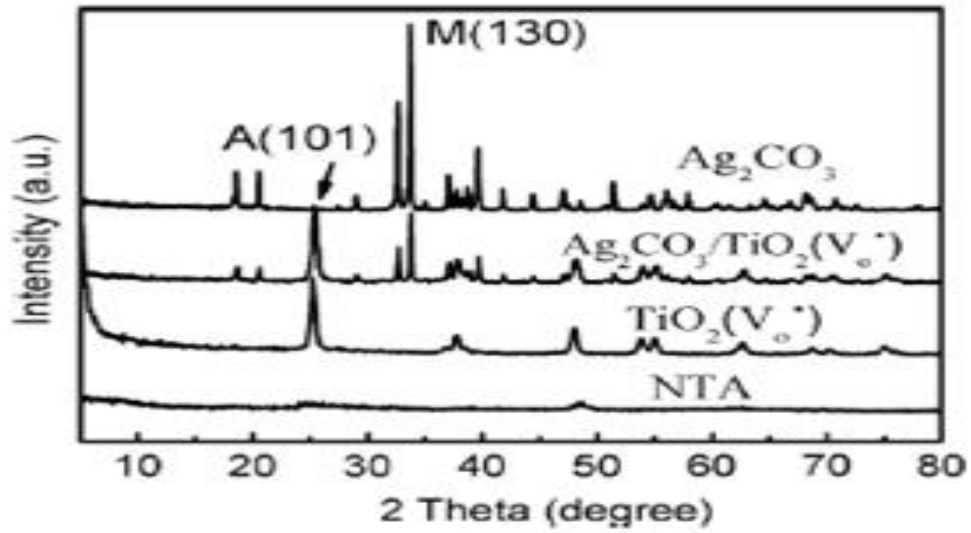


Fig.2 XRD Patterns of NTA, $\text{TiO}_2(\text{V}_o^*)$, and $\text{Ag}_2\text{CO}_3/\text{TiO}_2(\text{V}_o^*)$,

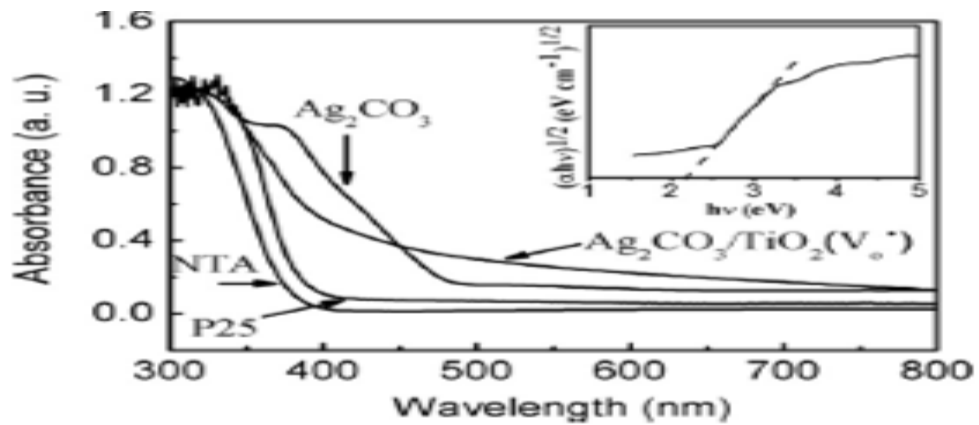


Fig.3 Diffuse reflectance spectra of NTA , P25, Ag_2CO_3 and $\text{Ag}_2\text{CO}_3/\text{TiO}_2(\text{V}_o^*)$

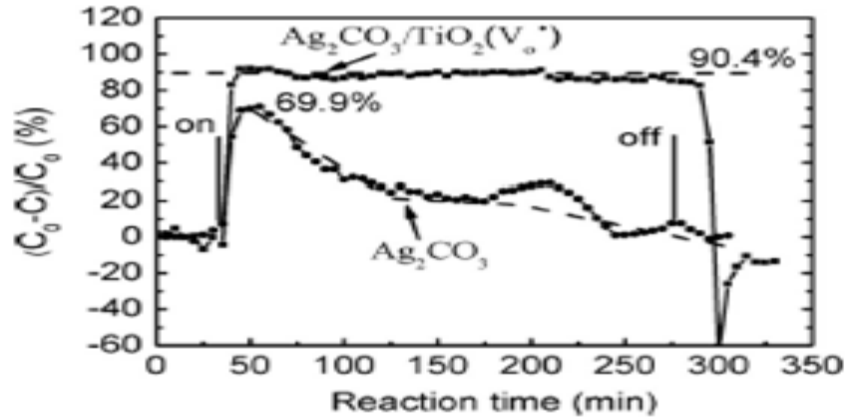


Fig.4 Photocatalytic degradation rate of propylene over, Ag_2CO_3 and $\text{Ag}_2\text{CO}_3/\text{TiO}_2(\text{V}_\text{o}^*)$ under visible light irradiation as a function of reaction time

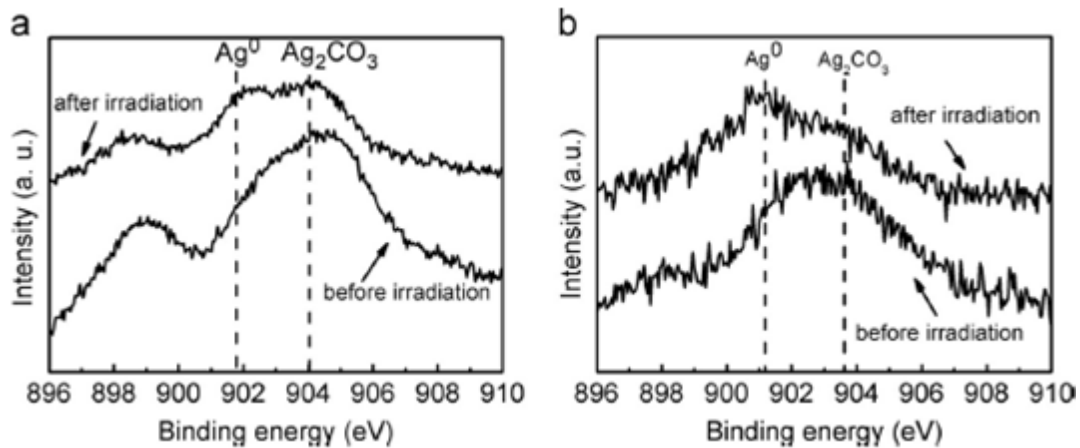


Fig.5 Auger Ag MNN XPS spectra of a) $\text{Ag}_2\text{CO}_3/\text{TiO}_2(\text{V}_\text{o}^*)$ b) before and after visible light irradiation

$\text{TiO}_2(\text{V}_\text{o}^*)$ must play an important role in enhancing the visible light photocatalytic activity of $\text{Ag}_2\text{CO}_3/\text{TiO}_2(\text{V}_\text{o}^*)$.

A large amount of SETOVs formed in a TiO_2 matrix can extend the absorption range of TiO_2 from ultraviolet region to visible light region, but they are inactive for visible light photocatalytic activity, because SETOVs, via interaction, may act as recombination centers of photogenerated $e^- - h^+$. However, TiO_2 doped with N shows apparent visible light photocatalytic activity, which is attributed to the synergistic effect between SETOVs and doped N.

This enlightens us that the excellent visible light photocatalytic performance of $\text{Ag}_2\text{CO}_3/\text{TiO}_2(\text{Vo})$ could be ascribed to the combination of Ag_2CO_3 with $\text{TiO}_2(\text{Vo})$. Namely Ag_2CO_3 in $\text{Ag}_2\text{CO}_3/\text{TiO}_2(\text{Vo})$ is excited to generate $e^- \cdot h^+$ pairs under visible light irradiation thereby initiating photocatalytic oxidation of propylene, while photo-corrosion of Ag_2CO_3 results in nascent metallic Ag on the surface of $\text{TiO}_2(\text{Vo})$. Although photo-corrosion of Ag_2CO_3 is originally not conducive to the visible light photo-catalytic activity of $\text{Ag}_2\text{CO}_3/\text{TiO}_2(\text{Vo})$, its photo-corrosion product, nascent metallic Ag, can be dispersed on the surface of $\text{TiO}_2(\text{Vo})$ in association with SETOVs in $\text{TiO}_2(\text{Vo})$ matrix to result in additional visible light photocatalytic activity of $\text{Ag}_2\text{CO}_3/\text{TiO}_2(\text{Vo})$. As a result, the gradually reduced visible light photocatalytic activity of $\text{Ag}_2\text{CO}_3/\text{TiO}_2(\text{Vo})$ owing to photo-corrosion of Ag_2CO_3 is compensated by nascent metallic Ag dispersed on the surface of $\text{TiO}_2(\text{Vo})$ and SETOVs already existed in $\text{TiO}_2(\text{Vo})$ matrix.

Conclusion

Visible-light-active Ag_2CO_3 and $\text{Ag}_2\text{CO}_3/\text{TiO}_2(\text{Vo})$ were prepared via a simple precipitation method. As-prepared photocatalysts were characterized by means of TEM, XRD, DRS, ESR and Auger MNN XPS. Both Ag_2CO_3 and $\text{Ag}_2\text{CO}_3/\text{TiO}_2(\text{Vo})$ exhibit highly photocatalytic activity towards the degradation of propylene under visible light irradiation. However, Ag_2CO_3 is unstable owing to photo-corrosion, and hence its visible light photocatalytic activity gradually declines with extending reaction time. Differing from Ag_2CO_3 , $\text{Ag}_2\text{CO}_3/\text{TiO}_2(\text{Vo})$ displays high and stable visible light photocatalytic activity of ca. 90.4% for the photo-oxidation of propylene. The reason may lie in that nascent metallic Ag formed from photo-corrosion of Ag_2CO_3 and the SETOVs in $\text{TiO}_2(\text{Vo})$ matrix jointly function to yield additional visible light photocatalytic activity thereby compensating for the gradually reduced visible light photocatalytic activity due to photo-corrosion of Ag_2CO_3 .

Reference

- [1] Xu CW, Liu YY, Huang BB, Li H, Qin XY, Zhang XY, et al. *Appl Surf Sci* 2011;257:8732–6.
- [2] Yan Wang Pin hong Ren a, Caixia Feng a, Xi Zheng a, Zigui Wang a, Deliang Li et al *Materials Letters* 115(2014)85–88
- [2] Dai GP, Yu JG, Liu G. *J Phys Chem C*2012; 116:15519–24.